Supporting Information

Water- Surface reconstruction of sulfurized spinel-structured oxide oxygen catalysts for alkaline water electrolysis

Sungyong Choi [a], Swetarekha Ram [b], Sung Ryul Choi [a], Won Young An [a], Seojeong Yoo [a], Seung-Cheol Lee [b], Satadeep Bhattacharjee [b,*], Jun-Young Park [a,*]

[a] *HMC, Department of Nanotechnology and Advanced Materials Engineering, Sejong University, Seoul 05006, Korea*

[b] *Indo Korea Science and Technology Center, Bangalore 560012, India*

* Correspondence and requests for materials should be addressed to **J.-Y. Park** (email: jyoung@sejong.ac.kr; Tel: +82-2-3408-3848) and **Satadeep Bhattacharjee (**email: s.bhattacharjee@ikst.res.in).

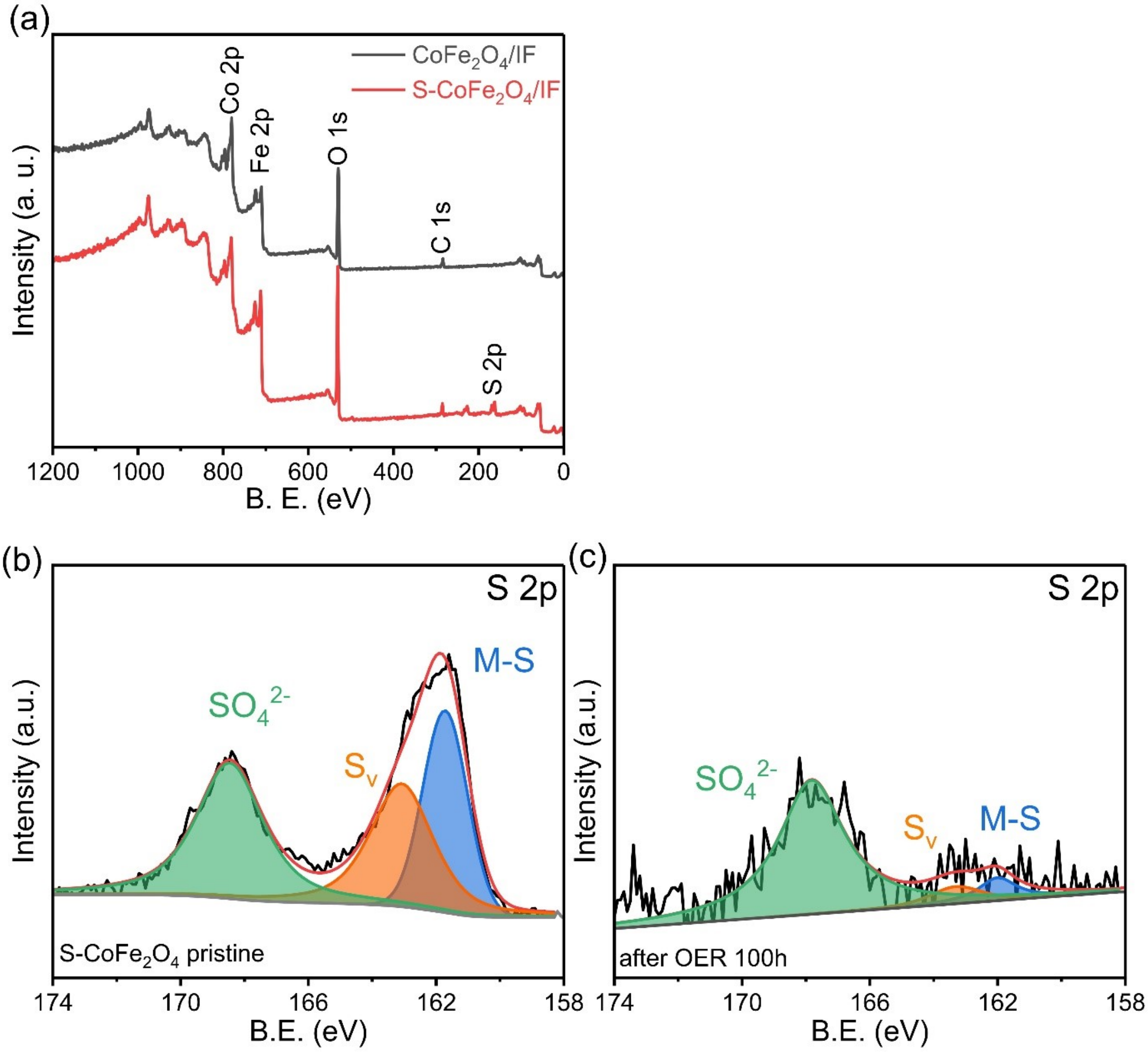

Fig. S1. (a) Full survey XPS spectra for $CoFe_2O_4$/IF and S-$CoFe_2O_4$/IF. (b–c) S 2p of S-$CoFe_2O_4$/IF before (b) and after OER durability test for 100 hours (c).

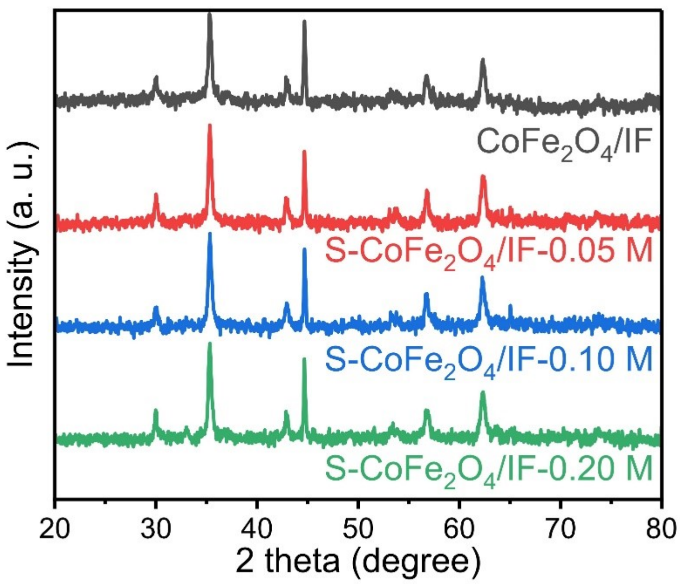

Fig. S2. XRD spectra for as-prepared $CoFe_2O_4$/IF and S-$CoFe_2O_4$/IF catalysts sulfurized with 0.05 M, 0.1 M, and 0.2 M Na_2S.

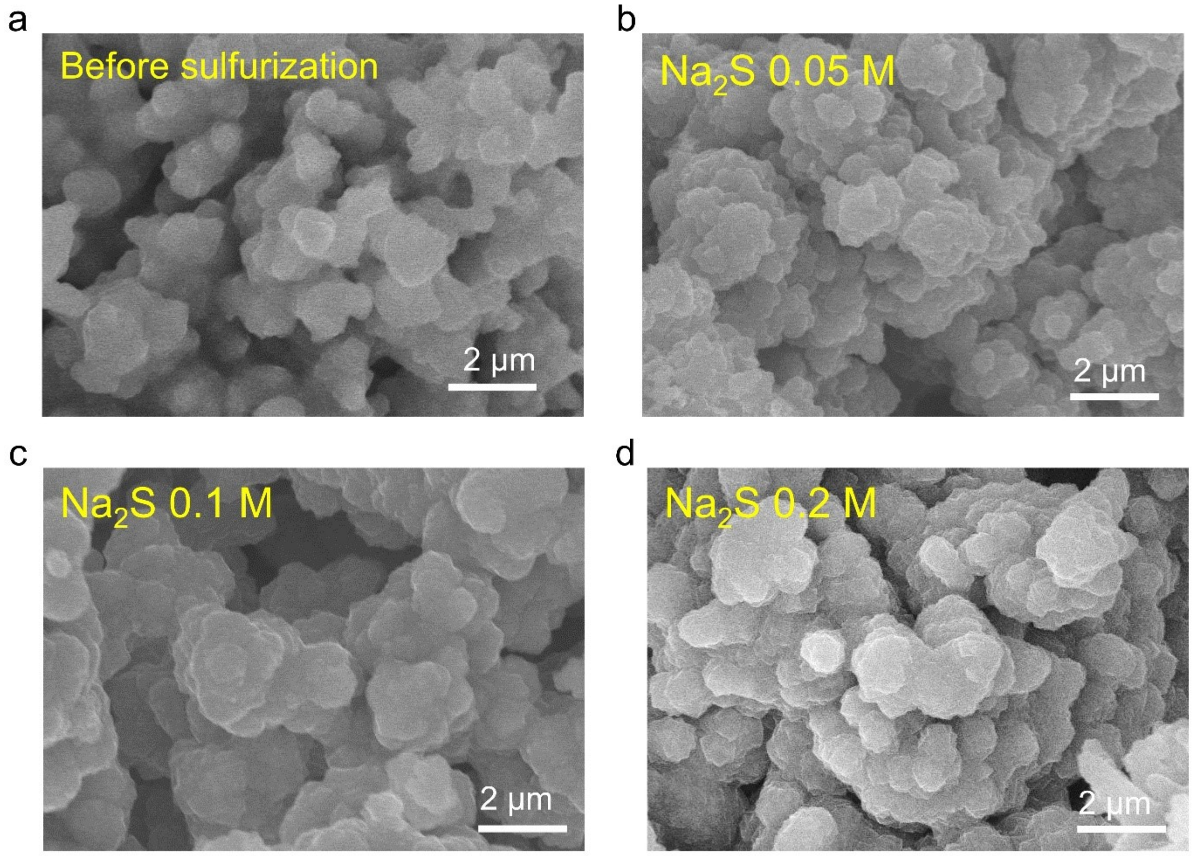

Fig. S3. FE-SEM images of $CoFe_2O_4$ and S-$CoFe_2O_4$ particles on iron foam. (a) Before sulfidation ($CoFe_2O_4$). (b) Sulfidation with 0.05 M Na_2S (S-$CoFe_2O_4$/IF-0.05). (c) Sulfidation with 0.1 M Na_2S (S-$CoFe_2O_4$/IF-0.1). (d) Sulfidation with 0.2 M Na_2S (S-$CoFe_2O_4$/IF-0.2).

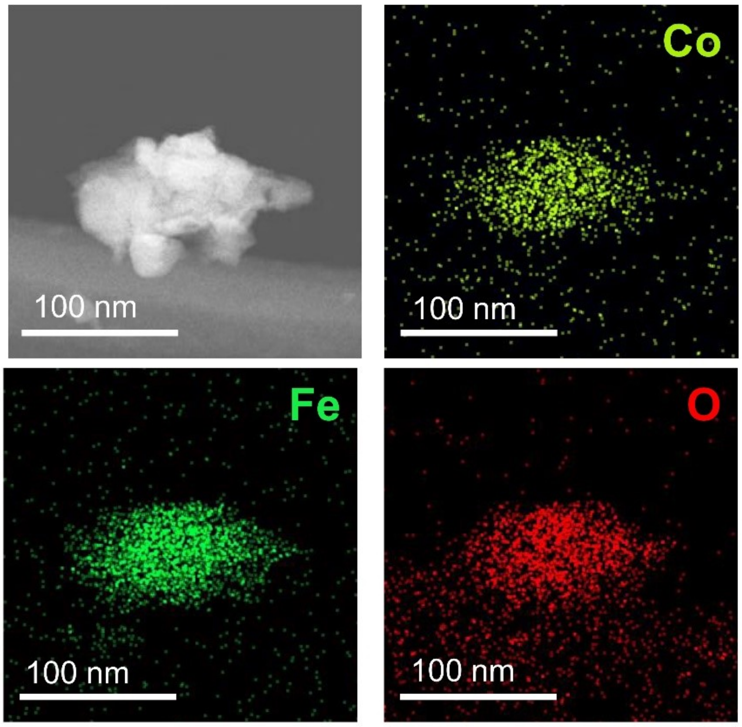

Fig. S4. TEM-EDX elemental mappings for as-prepared $CoFe_2O_4$/IF.

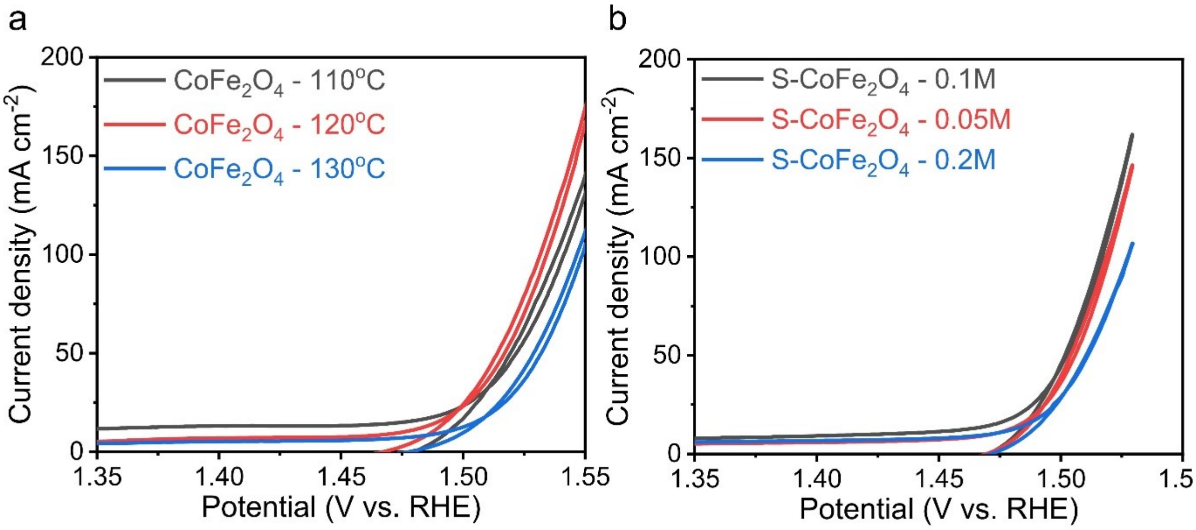

Fig. S5. (a) OER polarization curves of $CoFe_2O_4$/IF catalysts under various hydrothermal processing conditions. (b) OER activity curves of S-$CoFe_2O_4$/IF catalysts prepared with Na_2S solution at various concentrations.

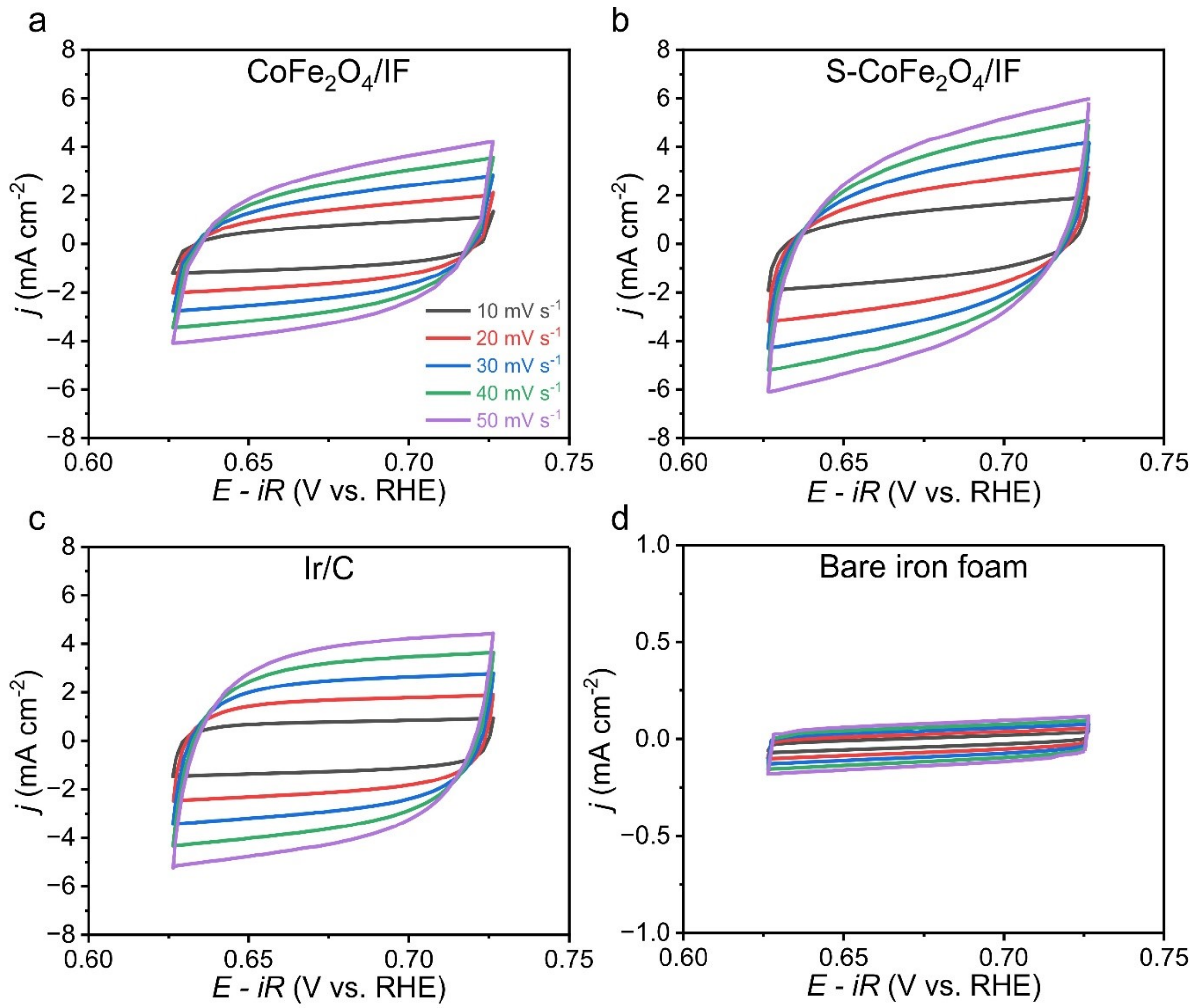

Fig. S6. Double-layer capacitance (C_{dl}) obtained from cyclic voltammograms (CVs, 0.625–0.725 V *vs.* RHE) of catalysts at various scan rates (10–50 mV·s^{-1}). (a) $CoFe_2O_4$/IF. (b) S-$CoFe_2O_4$/IF. (c) Ir/C. (d) Bare Fe foam.

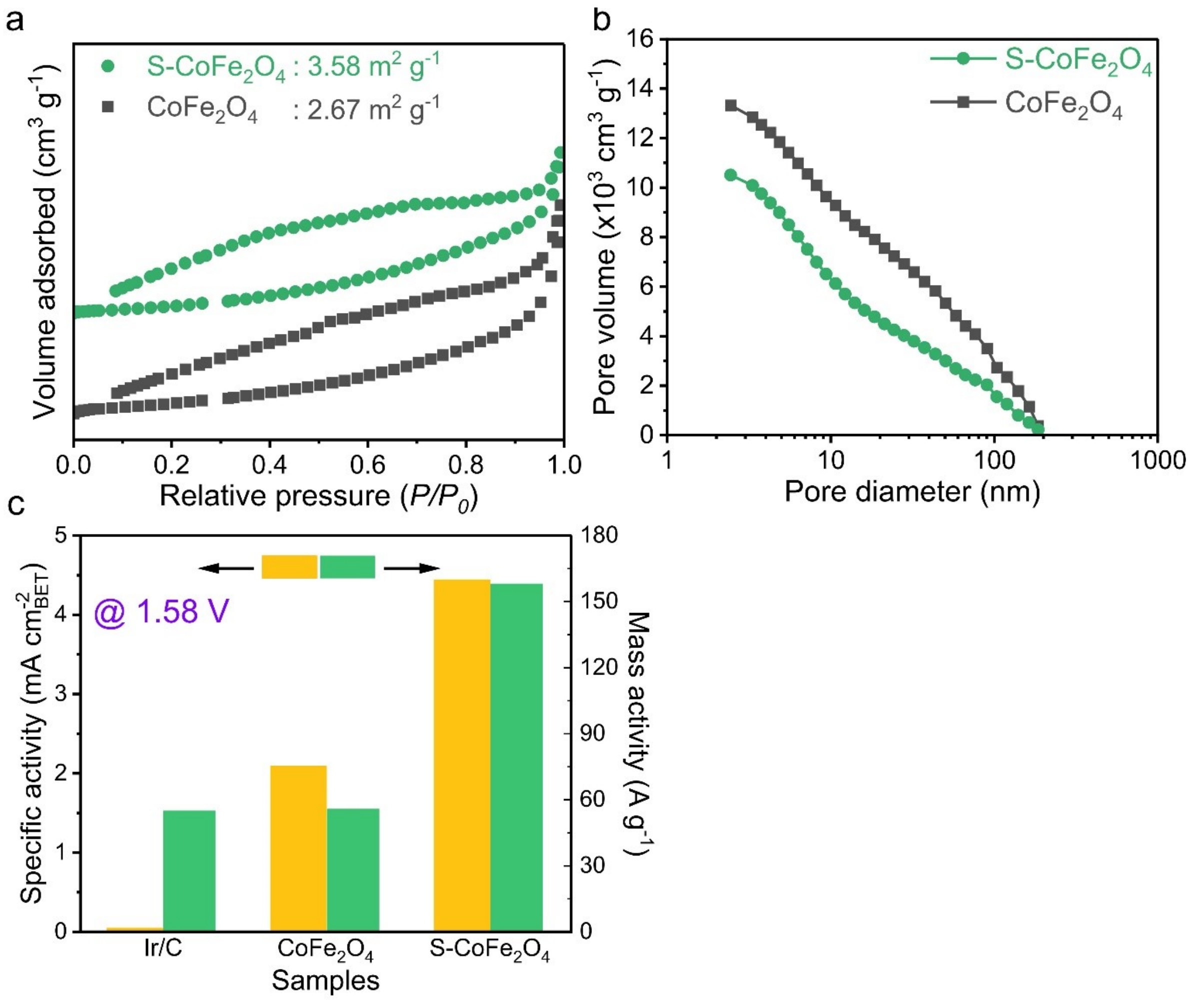

Fig. S7. Specific surface areas (Brunauer–Emmet–Teller, BET) and activities of Ir/C, $CoFe_2O_4$/IF, and S-$CoFe_2O_4$/IF catalysts. (a) Nitrogen adsorption-desorption isotherms. (b) Total pore volume and pore size. (c) Specific activities and mass activities of catalysts normalized by BET and loading mass.

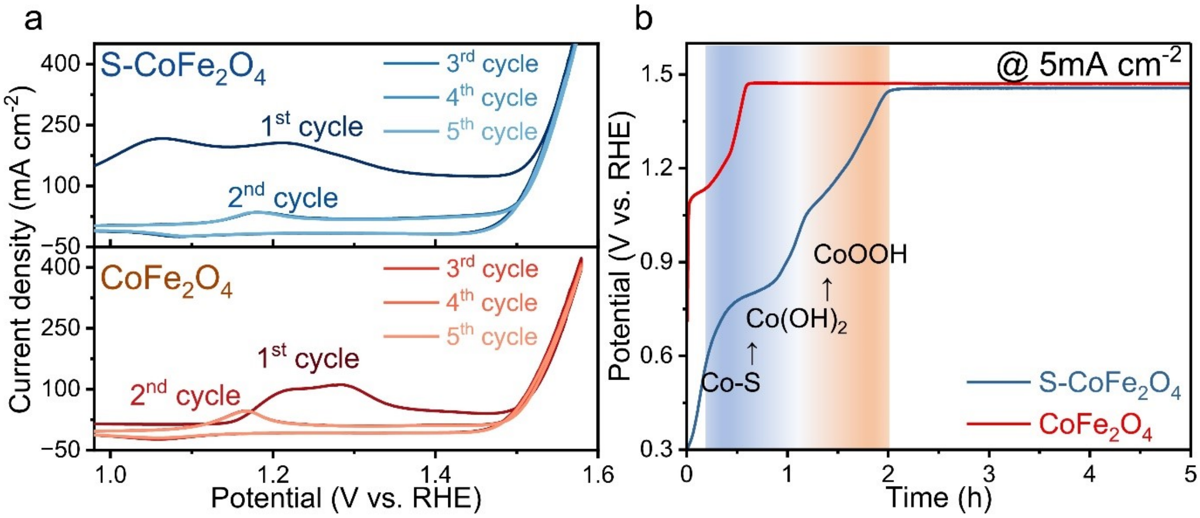

Fig. S8. Investigation of detailed surface reconstruction of catalysts. (a) The 1st to 5th CV cycles for OER of $CoFe_2O_4$/IF and S-$CoFe_2O_4$/IF in an O_2-saturated 1.0 M KOH. (b) Chronopotentiometry curve of S-$CoFe_2O_4$/IF at 5 $mA \cdot cm^{-2}$. No pre-electrochemical or activation treatment was applied.

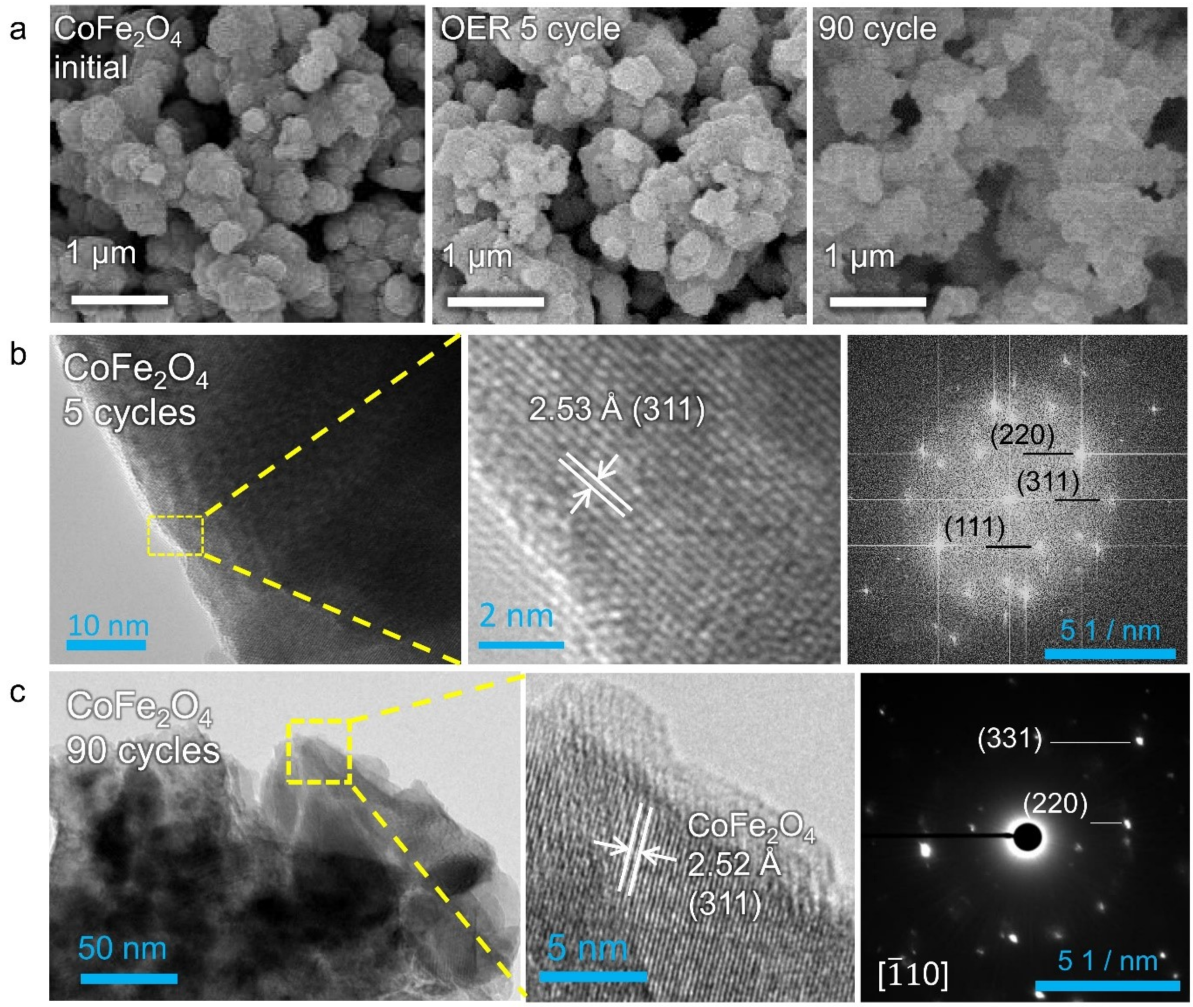

Fig. S9. Observation of surface reconstruction process of $CoFe_2O_4$/IF. (a) FE-SEM images before and after the 5th and 90th cycles of OER. (b) HR-TEM image and corresponding fast Fourier transform (FFT) patterns after the 5th cycle of OER. (c) HR-TEM image with SAED patterns after the 5th cycle of OER.

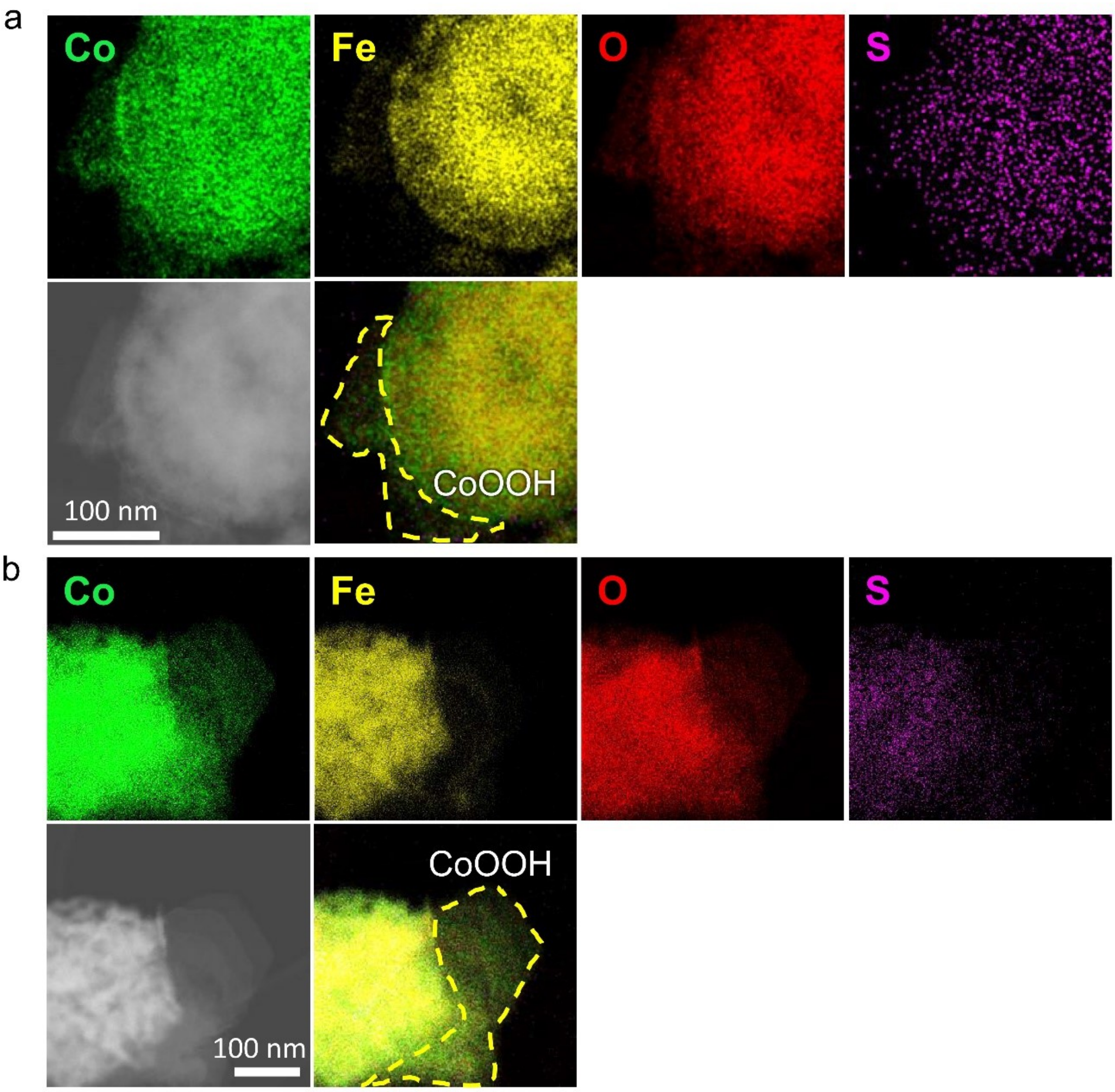

Fig. S10. TEM-EDX elemental mapping results of S-$CoFe_2O_4$/IF. a) After the 5th cycle of OER. b) After 100 hours of short-term OER stability test under 0.1 $A{\cdot}cm^{-2}$.

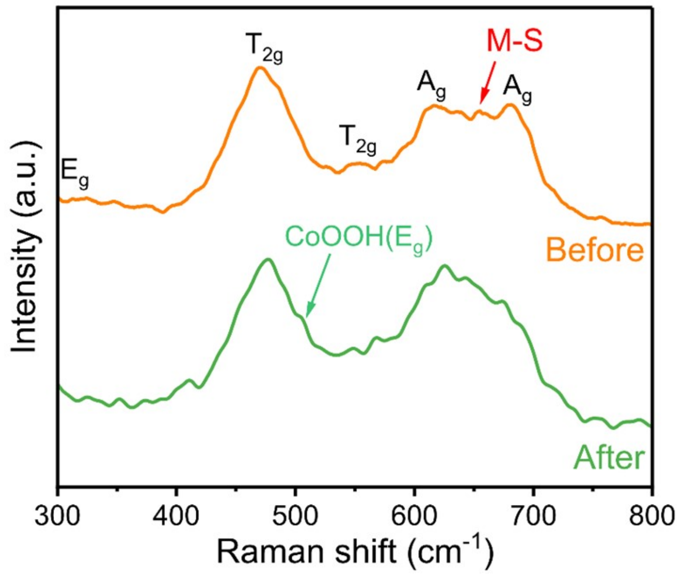

Fig. S11. Raman spectra of S-$CoFe_2O_4$/IF catalysts before and after OER tests for 20 hours.

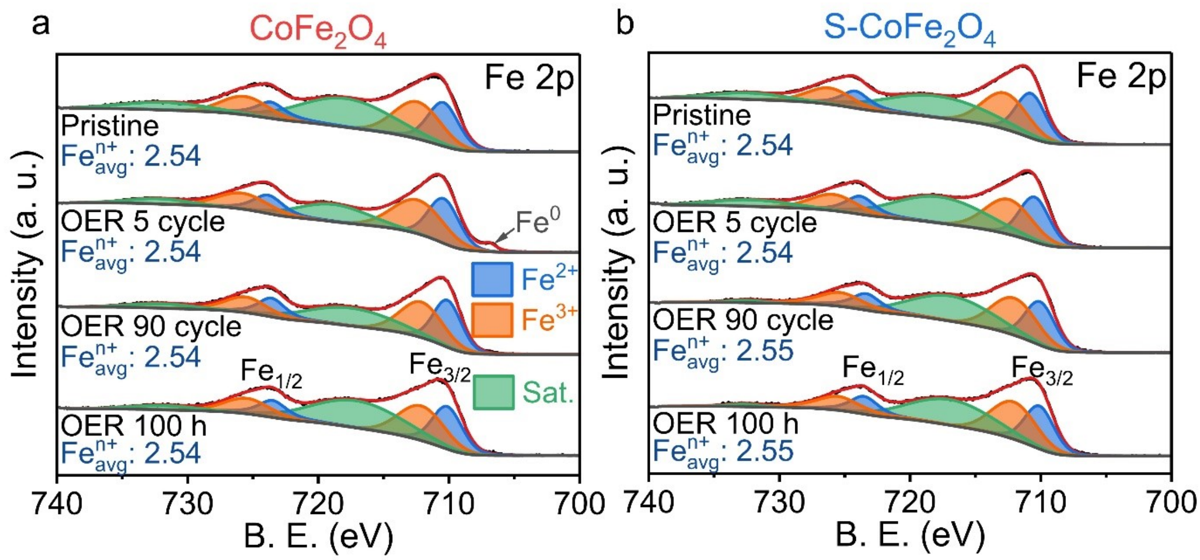

Fig. S12. Electronic structure modification of catalysts by XPS spectra during OER testing (pristine, 5th cycles, 90th cycles, constant current test under 0.1 A·cm^{-2} for 100 hours). (a) Fe 2p spectra of $CoFe_2O_4$/IF. (b) Fe 2p spectra of S-$CoFe_2O_4$/IF.

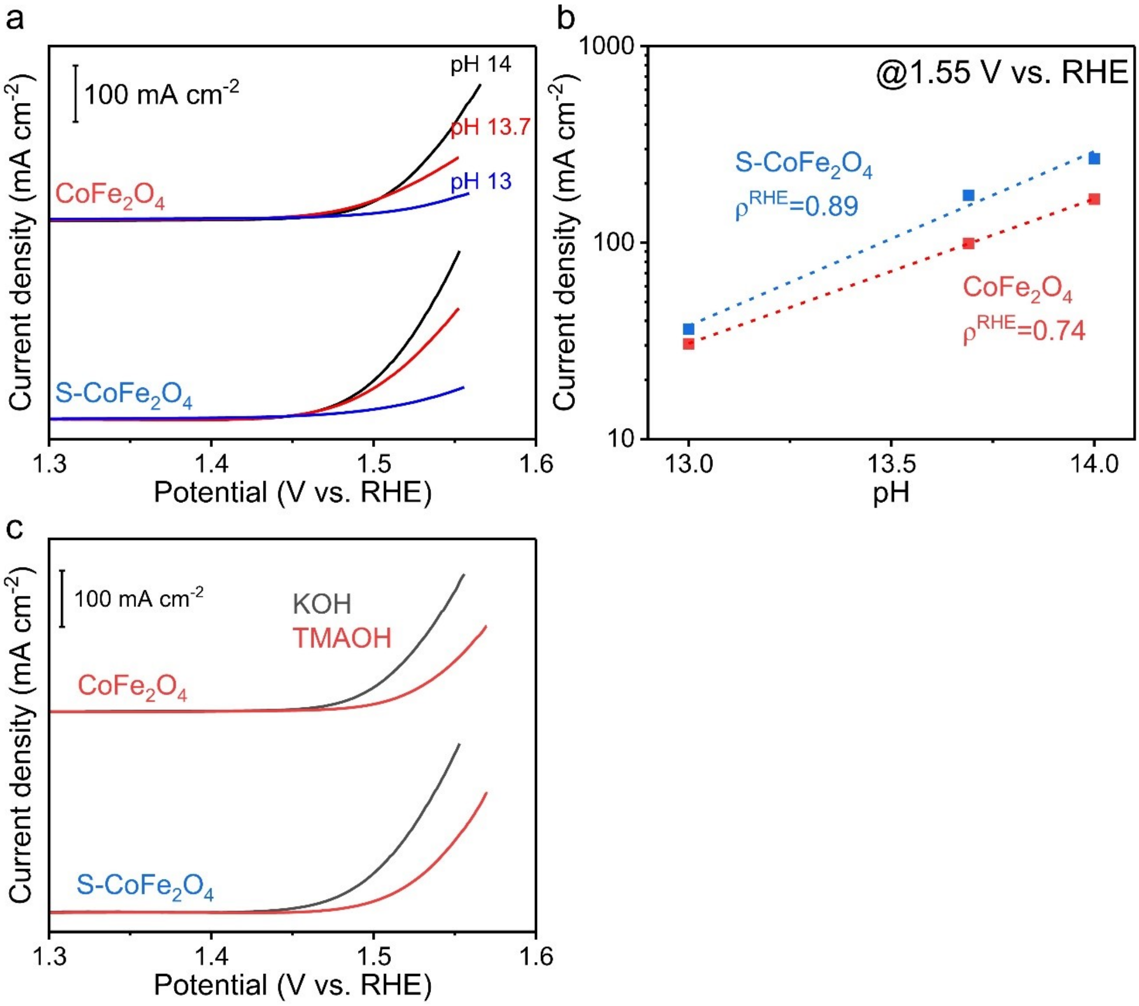

Fig. S13. Understanding of the OER reaction mechanism for $CoFe_2O_4$/IF and S-$CoFe_2O_4$/IF. (a) Linear sweep voltammetry measurement from 0.1 (pH 13) to 1.0 M KOH (pH 14) recorded at 10 mV·s^{-1}. (b) pH dependent OER activity on RHE scale at 1.55 V vs. RHE. (c) Polarization curves in 1 M KOH and TMAOH electrolytes.

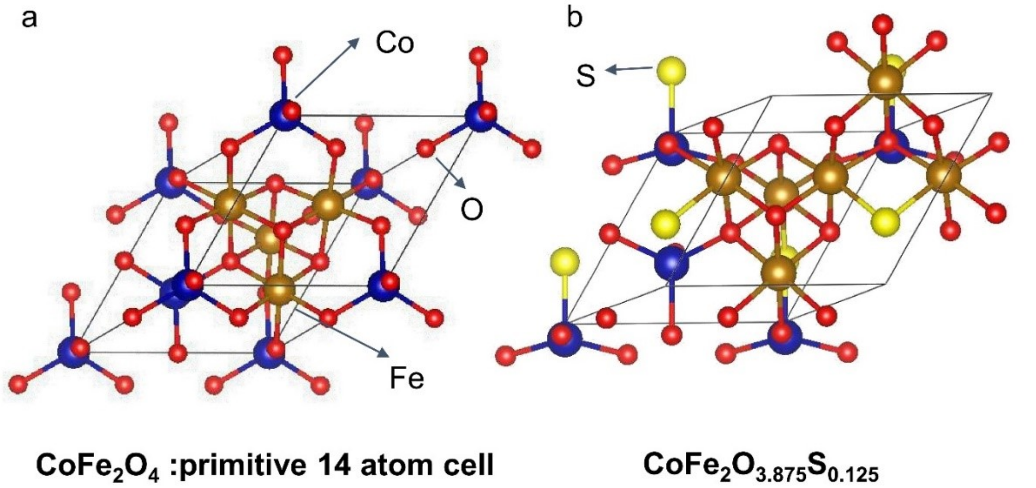

Fig. S14. Elucidation of distinct origin of the superior OER performance based on density functional theory (DFT) calculations. (a) Pure $CoFe_2O_4$ structure. (b) Structure considered to model S-$CoFe_2O_4$.

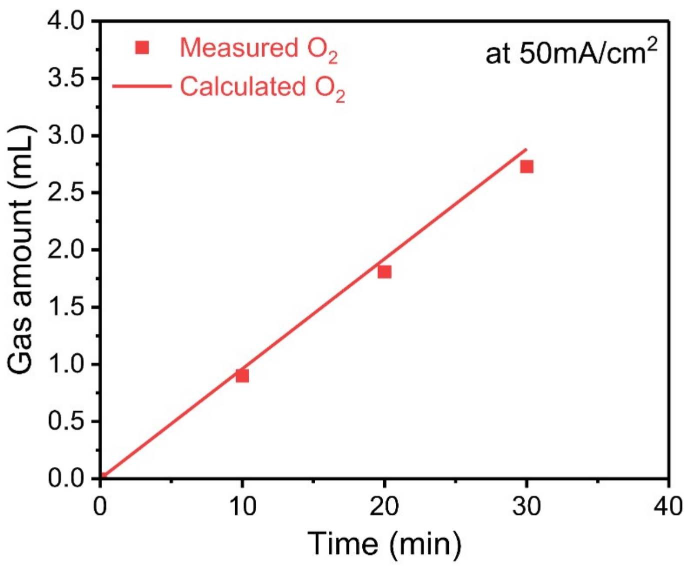

Fig. S15. The correlation between the amount of O_2 gas evolved and the duration of water splitting using the S-$CoFe_2O_4$ electrocatalyst.

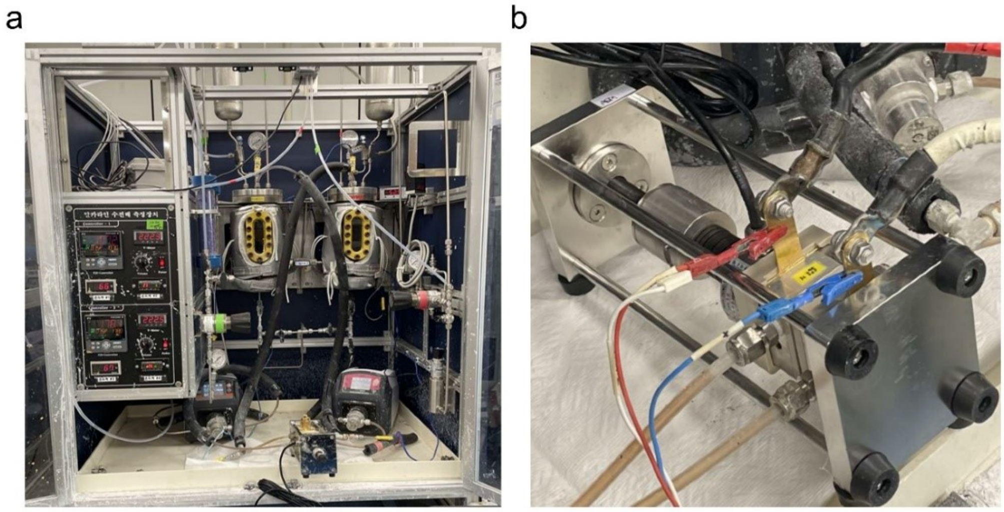

Fig. S16. Experimental setup of alkaline exchange membrane water electrolysis (AEMWE) cells. (a) Automatic cell test-station. (b) Cell test hardware.

Table S1. Degree of sulfidation (S atomic ratio normalized to Fe and Co contents) of catalysts estimated using ICP analysis.

Catalysts	**Co**	**Fe**	**S**
	at.%	at.%	at%
$CoFe_2O_4$/IF	10.1	89.4	**0**
S-$CoFe_2O_4$/IF-0.05	8.3	89.7	**2.0**
S-$CoFe_2O_4$/IF-0.1	8.7	88.8	**2.6**
S-$CoFe_2O_4$/IF-0.2	9.4	87.5	**3.0**
S-$CoFe_2O_4$/IF-0.1 (After 120 OER cycles)	7.8	90.6	**1.6**

Table S2. Characterization data of $CoFe_2O_4$/IF and S-$CoFe_2O_4$/IF catalysts obtained from N_2 adsorption analysis.

Catalyst	**BET surface area ($m^2 \cdot g^{-1}$)**	**Mean pore diameter (nm)**	**Total pore volume ($cm^3 \cdot g^{-1}$)**
$CoFe_2O_4$/IF	2.67	18.5	0.012
S-$CoFe_2O_4$/IF	3.58	10.4	0.009

Table S3. Comparison of OER activities of $CoFe_2O_4$/IF and recently reported state-of-the-art electrocatalysts.

Catalyst	**η@0.1 A·cm^{-2} (V)**	**Tafel slope (mV·dec^{-1})**	**References**
S-$CoFe_2O_4$/IF	0.285	42.6	This work
NiFe-OOH@FeNi cloth	0.287	67	*Appl. Catal. B.,* 2021, **286**, 119902.
CoNi/$CoFe_2O_4$@NF	0.290	45	*J. Mater. Chem. A,* 2018, **6**, 19221-19230.
$MoFe_2O_4$NS@IF	0.291	41	*Adv. Sci.,* 2021, **8**, 2101653.
(NiCo)Fe-MOF@NF	0.291	41.3	*Adv. Mater.,* 2019, **31**, 1901139.
Ni-Fe/$NiMoN_x$@NF	0.292	39.2	*Catal. Commun.,* 2022, **164**, 106426.
FeS/Fe_2O_3@IF	0.294	51.2	*J. Alloys Compd.,* 2022, **909**, 164670.
CoFeN NSs	0.308	47	*Nano Energy,* 2019, **57**, 644-652.
$NiFe_{0.5}$Sn-A@CC	0.301	30	*Adv. Sci.,* 2020, **7**, 1903777.
$Fe_{0.33}Co_{0.67}$OOH PNSAs@CFC	0.301	50	*Angew. Chem. Int. Ed.,* 2018, **57**, 2672-2676.
$CoFe_2O_4$@NF	0.303	30	*Catalysts,* 2019, **9**, 176.
FeNiP@C	0.311	74.5	*Nano Energy,* 2019, **62**, 745-753.
Ag-CoOOH@Ag thin film	0.320	96.8	*Adv. Powder Technol.,* 2022, **33**, 103728.
CoFe@C	0.322	45.2	*Adv. Sci.,* 2019, **6**, 1900117.
Ni-CoOOH@NF	0.331	82.1	*J. Chem. Eng.,* 2022, **443**, 136432.
CoFe-P@NF	0.336	43.2	*J. Colloid Interface Sci.,* 2022, **622**, 250-260.
NiO@CN	0.35	58.9	*Adv. Funct. Mater.,* 2019, **29**, 1904020.
Co_3O_4/CoFe	0.361	61	*Adv. Mater.,* 2018, **30**, 1801211.
$FeCo_2O_4$/$FeCo_2S_4$/PPy-12@NF	0.378	65.1	*Nano Energy,* 2020, **72**, 104715.
$CoFeP_x$	0.390	58	*Nano Energy,* 2019, **63**, 103855.
CoFePO@NF	0.417	51.7	*ACS Nano,* 2016, **10**,

			8738-8745.
NiFe foam	0.390	56	*Int. J. Hydrog. Energy.*, 2015, **40**, 13258-13263.
W-Co_V-CoOOH@NF	0.311	46.1	*Adv. Mater.*, 2022, **34**, 2104667.
NiCo-LDH@NF	0.370	72	*Dalton Trans.*, 2017, **46**, 8372-8376.
Fe-Co_9S_8@NF	0.351	70	*Appl. Surf. Sci.*, 2018, **454**, 46-53.
NNF-D	0.300	60.06	*Small,* 2024, 2400046.
FeS_2/MS/NF	0.314	60	*Appl. Catal., B,* 2023, **339**, 123171.
S-FeOOH/IF	0.308	59	*Adv. Funct. Mater.*, 2022, **32**, 2112674.

Table S4. Charge transfer analysis through Bader charge.

$CoFe_2O_4$			**$CoFe_2S_4$**			**$CoFe_2(O_{0.875}S_{0.125})_4$**		
Bond length (Å)		**Bader**	**Bond length (Å)**		**Bader**	**Bond length (Å)**		**Bader**
Co-Co	3.5	Co= +1.25 Fe= +1.74 O= –1.18	Co-Co	4.36	Co= +0.93 Fe= +1.27 O= –0.86	Co-Co	3.27	Co*-S= +1.18 Co*-O= +1.32 Fe*-S= +1.65 Fe*-O= +1.76 S= –0.83 O= –1.21~ –1.19
Co-O	1.9		Co-O	2.31		Co-S	2.2	
Fe-O	1.94		Fe-O	2.44		Fe-S	2.35	
Fe-Fe	2.87		Fe-Fe	3.56		Fe-Fe	2.97	
						Fe-O	2.04	
						Co-O	1.98	

OER mechanisms:

We applied a Mars van Krevelen-type mechanism[28] to investigate the free energy of the OER reaction. According to this mechanism, instead of OH adsorption, the reaction commences with the deprotonation of the surface OH on the in-situ surface phase. The reaction mechanism for OER in alkaline medium is as follows:

$$OH^* + OH^- \rightarrow O_L^* + H_2O + e^- \quad (1)$$

$$O_L^* + H_2O + OH^- \rightarrow O_LOH^* + H_2O + e^- \quad (2)$$

$$O_LOH^* + H_2O + OH^- \rightarrow O_LO^* + 2H_2O + e^- \quad (3)$$

$$O_LO^* + 2H_2O \rightarrow O_2(g) + 2H_2O + \mathrm{V} \quad (4)$$

$$V + 2H_2O + OH^- \rightarrow * + 2H_2O + e^- \quad (5)$$

The corresponding reaction mechanism for OER in acidic medium is as follows:

$$OH^* \rightarrow O_L^* + (H^+ + e^-) \quad (6)$$

$$O_L^* + H_2O \rightarrow O_LOH^* + (H^+ + e^-)$$

(7)

$$O_LOH^* \rightarrow O_LO^* + (H^+ + e^-) \quad (8)$$

$$O_LO^* \rightarrow O_2(g) + \mathrm{V} \quad (9)$$

$$V + H_2O \rightarrow * + (H^+ + e^-) \quad (10)$$

This mechanism involves the dehydrogenation of the initial hydroxyl group (OH*) through the removal of the proton and electron, resulting in the formation of a lattice oxygen, O_L^* and a vacancy (V) on the catalyst due to O_2 evolution. The catalyst is then regenerated by the adsorption of an H_2O molecule and subsequent dehydrogenation. The non-electrochemical step in equation (9) is followed by the electrochemical processes, which include the exchange of protons and electrons.

The adsorption free energy was calculated as follows:

$$\Delta G = \Delta E + \Delta ZPE - T\Delta S - neU \quad (11)$$

where ΔZPE represents the change in zero-point energy and ΔE is the change in structural energy, both computed according to earlier studies[29]. Room temperature (298.15 K) is represented by T, the charge constant (e), the number of electrons (n), the change in entropy (ΔS), and the overpotential (U). With a maximum reaction free energy barrier of 1.71 eV, an overpotential (η_{OER}) of 0.48 V (η_{OER} =1.7 – 1.23) eV/e^- is predicted (Table S5). The highest free energy barrier occurs during the deprotonation of OH^* in the OER cycle, resulting in the formation of ${O_L}^*$. Hence, this step seems to be the potential limiting step, after which O_2 is evolved by deprotonation.

Table S5. Reaction Gibbs free energy (ΔG) of OER and the overpotential (η_{OER}) of CoOOH/S-$CoFe_2O_4$.

Reaction	η_{OER} (V)	η_{OER} (V)
$OH^* \rightarrow {O_L}^* + (H^+ + e^-)$	**1.71**	0.48
${O_L}^* + H_2O \rightarrow O_LOH^* + (H^+ + e^-)$	1.54	
$O_LOH^* \rightarrow O_LO^* + (H^+ + e^-)$	0.97	
$O_LO^* \rightarrow O_2(g) +$ V	1.61	
$V + H_2O \rightarrow * + (H^+ + e^-)$	–1.42	

References

1. G. Zhang, J. Zeng, J. Yin, C. Zuo, P. Wen, H. Chen, Y. Qiu, Iron-facilitated surface reconstruction to in-situ generate nickel–iron oxyhydroxide on self-supported FeNi alloy fiber paper for efficient oxygen evolution reaction, *Appl. Catal. B.*, 2021, **286**, 119902.
2. S. Li, S. Sirisomboonchai, A. Yoshida, X. An, X. Hao, A. Abudula, G. Guan, Bifunctional CoNi/$CoFe_2O_4$ /Ni foam electrodes for efficient overall water splitting at a high current density, *J. Mater. Chem. A*, 2018, **6**, 19221-19230.
3. X. Yue, X. Qin, Y. Chen, Y. Peng, C. Liang, M. Feng, X. Qiu, M. Shao, S. Huang, Constructing active sites from atomic-scale geometrical engineering in spinel oxide solid solutions for efficient and robust oxygen evolution reaction electrocatalysts, *Adv. Sci.*, 2021, **8**, 2101653.
4. Q. Qian, Y. Li, Y. Liu, L. Yu, G. Zhang, Ambient fast synthesis and active sites deciphering of hierarchical foam-like trimetal–organic framework nanostructures as a platform for highly efficient oxygen evolution electrocatalysis, *Adv. Mater.*, 2019, **31**, 1901139.
5. Y. Qiu, M. Sun, J. Cheng, J. Sun, D. Sun, L. Zhang, Bifunctional Ni-Fe/$NiMoN_x$ nanosheets on Ni foam for high-efficiency and durable overall water splitting, *Catal. Commun.*, 2022, **164**, 106426.
6. W.H. Guo, Q. Zhang, H.C. Fu, Y.X. Yang, X.H. Chen, H.Q. Luo, N.B. Li, Semi-sacrificial template growth of FeS/Fe_2O_3 heterogeneous nanosheets on iron foam for efficient oxygen evolution reaction, *J. Alloys Compd.*, 2022, **909**, 164670.
7. L. An, J. Feng, Y. Zhang, Y.-Q. Zhao, R. Si, G.-C. Wang, F. Cheng, P. Xi, S. Sun, Controllable tuning of Fe-N nanosheets by Co substitution for enhanced oxygen evolution reaction, *Nano Energy*, 2019, **57**, 644-652.

8. M. Chen, S. Lu, X.-Z. Fu, J.-L. Luo, Core–Shell structured NiFeSn@NiFe (oxy)hydroxide nanospheres from an electrochemical strategy for electrocatalytic oxygen evolution reaction, *Adv. Sci.*, 2020, **7**, 1903777.

9. S.-H. Ye, Z.-X. Shi, J.-X. Feng, Y.-X. Tong, G.-R. Li, Activating CoOOH porous nanosheet arrays by partial iron substitution for efficient oxygen evolution reaction, *Angew. Chem. Int. Ed.*, 2018, **57**, 2672-2676.

10. C. Zhang, S. Bhoyate, C. Zhao, P.K. Kahol, N. Kostoglou, C. Mitterer, S.J. Hinder, M.A. Baker, G. Constantinides, K. Polychronopoulou, C. Rebholz, R.K. Gupta, Electrodeposited nanostructured $CoFe_2O_4$ for overall water splitting and supercapacitor applications, *Catalysts*, 2019, **9**, 176.

11. X. Wang, L. Chai, J. Ding, L. Zhong, Y. Du, T.-T. Li, Y. Hu, J. Qian, S. Huang, Chemical and morphological transformation of MOF-derived bimetallic phosphide for efficient oxygen evolution, *Nano Energy*, 2019, **62**, 745-753.

12. R. Zhang, Z. Hu, W. Ke, M. He, T. Ning, J. Bao, Z. Shang, W. Zhu, G. Zhu, Plasmon-promoted oxygen evolution catalysis with Ag nanocrystals loaded α-$Co(OH)_2$ nanosheets, *Adv. Powder Technol.*, 2022, **33**, 103728.

13. J. Du, G. Liu, F. Li, Y. Zhu, L. Sun, Iron–salen complex and Co^{2+} ion-derived cobalt–iron hydroxide/carbon nanohybrid as an efficient oxygen evolution electrocatalyst, *Adv. Sci.*, 2019, **6**, 1900117.

14. M. Chen, D. Liu, J. Feng, P. Zhou, L. Qiao, W. Feng, Y. Chen, K. Wei Ng, S. Wang, W. Fai Ip, H. Pan, In-situ generation of Ni-CoOOH through deep reconstruction for durable alkaline water electrolysis, *J. Chem. Eng.*, 2022, **443**, 136432.

15. D. Duan, D. Guo, J. Gao, S. Liu, Y. Wang, Electrodeposition of cobalt-iron bimetal phosphide on Ni foam as a bifunctional electrocatalyst for efficient overall water splitting, *J. Colloid Interface Sci.*, 2022, **622**, 250-260.

16. C. Liao, B. Yang, N. Zhang, M. Liu, G. Chen, X. Jiang, G. Chen, J. Yang, X. Liu, T.-S. Chan, Y.-J. Lu, R. Ma, W. Zhou, Constructing conductive interfaces between nickel oxide nanocrystals and polymer carbon nitride for efficient electrocatalytic oxygen evolution reaction, *Adv. Funct. Mater.*, 2019, **29**, 1904020.

17. X. Wang, L. Yu, B.Y. Guan, S. Song, X.W. Lou, Metal–organic framework hybrid-assisted formation of Co_3O_4/Co-Fe oxide double-shelled nanoboxes for enhanced oxygen evolution, *Adv. Mater.*, 2018, **30**, 1801211.

18. D. Zhao, M. Dai, Y. Zhao, H. Liu, Y. Liu, X. Wu, Improving electrocatalytic activities of $FeCo_2O_4$@$FeCo_2S_4$@PPy electrodes by surface/interface regulation, *Nano Energy*, 2020, **72**, 104715.

19. C. Yang, M. Cui, N. Li, Z. Liu, S. Hwang, H. Xie, X. Wang, Y. Kuang, M. Jiao, D. Su, L. Hu, In situ iron coating on nanocatalysts for efficient and durable oxygen evolution reaction, *Nano Energy*, 2019, **63**, 103855.

20. J. Duan, S. Chen, A. Vasileff, S.Z. Qiao, Anion and cation modulation in metal compounds for bifunctional overall water splitting, *ACS Nano*, 2016, **10**, 8738-8745.

21. Y. Liang, Q. Liu, A.M. Asiri, X. Sun, Y. He, Nickel–iron foam as a three-dimensional robust oxygen evolution electrode with high activity, *Int. J. Hydrog. Energy.*, 2015, **40**, 13258-13263.

22. Y. Dou, D. Yuan, L. Yu, W. Zhang, L. Zhang, K. Fan, M. Al-Mamun, P. Liu, C.-T. He, H. Zhao, Interpolation between W dopant and Co vacancy in CoOOH for enhanced oxygen evolution catalysis, *Adv. Mater.*, 2022, **34**, 2104667.

23. W. Liu, J. Bao, M. Guan, Y. Zhao, J. Lian, J. Qiu, L. Xu, Y. Huang, J. Qian, H. Li, Nickel–cobalt-layered double hydroxide nanosheet arrays on Ni foam as a bifunctional electrocatalyst for overall water splitting, *Dalton Trans.*, 2017, **46**, 8372-8376.
24. W.-K. Gao, J.-F. Qin, K. Wang, K.-L. Yan, Z.-Z. Liu, J.-H. Lin, Y.-M. Chai, C.-G. Liu, B. Dong, Facile synthesis of Fe-doped Co_9S_8 nano-microspheres grown on nickel foam for efficient oxygen evolution reaction, *Appl. Surf. Sci.*, 2018, **454**, 46-53.
25. J.-H. Park, H. J. Kwon, D. Y. Lee, S.-J. Suh, Effect of Ni sulfate residue on oxygen evolution reaction (OER) in porous NiFe@NiFe layered double hydroxide, *Small*, 2024, 2400046.
26. C. Yue, X. Zhang, J. Yin, H. Zhou, K. Liu, X. Liu, Highly efficient FeS_2@FeOOH core-shell water oxidation electrocatalyst formed by surface reconstruction of FeS_2 microspheres supported on Ni foam, *Appl. Cat. B*, 2023, **339**, 123171.
27. X. Chen, Q. Wang, Y. Cheng, H. Xing, J. Li, X. Zhu, L. Ma, Y. Li, D. Liu, S-doping triggers redox reactivities of both iron and lattic oxygen in FeOOH for low-cost and high-performance water oxidation, *Adv. Funct. Mater.*, 2022, **32**, 2112674.
28. I. Zegkinoglou, H. Sarodnik, D. Fan, A. Bergmann, In-situ structure and catalytic mechanism of NiFe and CoFe layered double hydroxides during oxygen evolution, *Nat. Comm.*, 2020, **11**, 2522.
29. J.K. Nørskov, J. Rossmeisl, A. Logadottir, L. Lindqvist, J.R. Kitchin, T. Bligaard, H. Jonsson, Origin of the overpotential for oxygen reduction at a fuel-cell cathode, *J. Phys. Chem. B*, 2004, **108**, 17886-17892.